

Decoherence Effects in Practical Quantum Cryptography Systems based on polarization entangled photons

S. Castelletto, I. P. Degiovanni, M. L. Rastello
Istituto Elettrotecnico Nazionale G. Ferraris
Strada delle Cacce 91-10135 Torino (Italy)

(Dated: May 21, 2019)

Quantum cryptography key distribution experiments (QCKD) have been recently based on polarization photon entanglement whose security is founded on its intrinsic quantum nature. Even though not in principle however in practical realization statistical noise, owing to decoherence effects induced by both photon source generation and measurement system, introduces a sort of degradation of quantum system performances.

In this paper, we investigate those effects inducing perturbation in the ideal polarization entanglement in spontaneous parametric downconversion (SPDC) and yielding errors in the transmitted bit sequence. Since all SPDC-based QCKD schemes rely on the measurement of coincidence to assert the bit transmission between the two parties, we developed a statistical model to calculate the density matrix of accidental coincidences. This model treats the outcoming statistical noise in QCKD system as a residual effect of decoherence due to the entanglement between the two-photons quantum system degrees of freedom, such as polarization and number of photon pairs, with the environment and the noisy and lossy measurement system.

This model predicts precisely the quantum bit error rate and the sifted key before and after error correction and guarantees a method to compare different security criteria of the hitherto proposed QCKD protocols, resulting in an objective assessment of performances and advantages of different systems.

PACS numbers: 42.50.-p, 42.50.Dv, 03.67.-a, 42.65.Ky.

I. INTRODUCTION

Quantum Cryptography Key Distribution (QCKD) is at the moment the most advanced and challenging application of the new field of quantum information. QCKD offers the possibility that two remote parties, sender and receiver (conventionally called Alice and Bob), exchange a secret random key, called sifted key (string of qubits), to implement a secure encryption/decryption algorithm based on a shared secret key, without the need that the two parties meet [1, 2, 3].

Practically in QCKD, Alice and Bob use a quantum channel, along which sequences of signals are sent/measured at random between different bases of orthogonal quantum states. Alice can play the role either of setting randomly the polarization basis of photons and send them to Bob (faint laser pulses as photon source), or of measuring photons randomly in anyone of the selected bases (entangled photon source). Bob, randomly and independently from Alice, measures in one of the basis. The sifted key consists of the subset of measurements performed when Alice's and Bob's bases are in an agreed configuration according to the protocol used, obtaining at this point a deterministic outcome whose security definitely relies on the laws of quantum physics, for they previously only agree on the correspondence between counting a photon in a specific state with the value of bit 0 or 1. By contrary the security of the conventional cryptography so far implemented is essentially relying over the unproven impossibility to factorize large numbers in prime numbers by a conventional algorithm, since up to

now there is no guarantee that such an algorithm does not exist.

The underlying feature of QCKD is therefore the definite advantage over the public key cryptography, to rely the security of the distributed secret key on the laws of quantum physics [1, 2, 3], in other words the uncertainty principle prohibiting to gain information from a quantum channel without disturbing it. Nevertheless this last claim must be somewhat softened because of practical realization of quantum channels [4]. Basically, QCKD is founded on the principle that, when a third party (Eve) performs a measurement on a qubit exchanged, she induces a perturbation yielding errors in the bit sequence transmitted and revealing her presence. Any attempt by Eve to obtain information about the key leads to a nonzero error rate in the generated sifted key. Unfortunately, in practical systems, errors also happen because of experimental leakage, like losses in optics, detection, electronics and noise. Also in the case of no eavesdropper disturbing the bit exchange, in practice there will be errors in the transmission thus Alice's and Bob's strings will not coincide perfectly. Since in practice there is no way to distinguish an eavesdropper attack from experimental imperfections, it is necessary to establish an upper bound on tolerable experimental imperfections in the realization of the quantum channels in order to allow error correction procedure.

Following the first proposal of Bennett and Brassard and, later, the Ekert protocol invoking entangled states, various systems of QCKD have been implemented and tested by groups around the world. In this trend, it is only recently that some research groups [5, 6, 7, 8, 9] per-

formed the first QCKD experiments based on polarization entangled photon pairs and Brassard *et al.* [4] proved theoretically that QCKD schemes based on spontaneous parametric down-conversion (SPDC) offer enhanced performances mostly in terms of security with respect to QCKD based on weak coherent pulses.

Entangled photons, generated by SPDC in nonlinear crystals, had been proved largely and successfully for optical measurements in fields regarded commonly as quantum optical communication [10, 11, 12, 13] and quantum radiometry [14, 15, 16, 17, 18, 19, 20, 21, 22, 23]. Furthermore basic experimental tests of the foundation of quantum mechanics had been abundantly performed by exploiting the entanglement of this source [24, 25, 26]. However decoherence in SPDC quantum state is a significant obstacle to the realization of proposed quantum optical communication and information technologies.

In this paper we provide a general model for an a priori evaluation of crucial parameters of a QCKD general scheme based on polarization entangled photons in terms of experimental imperfections present in quantum channels and/or in the measurement system, inducing an overall decoherence outcome.

In Section II we consider decoherence effects resulting in practical systems, due to the entanglement of the quantum system with the measurement system. Firstly, we discuss the case of lossless measurement system (Section III.A and B) and, secondly the case of an actual lossy and noisy measurement system (Section IV.A and B). In the former case the decoherence is owed both to the entanglement between the polarization mode of the source with the polarizing beam splitter ports, and to the entanglement between the photon number states with the detection system. For a lossy system the decoherence is induced by mere statistical noise due to detection deficiencies, such as losses of correlated photons for the presence of optical elements, non ideal detectors and electronic devices in either channels, and to detector dark counts (Section V).

The model ends up with the calculation of an overall density matrix of the coincidence counts, including also imperfect time correlation measurement, ultimately yielding an outcoming estimate of accidental coincidences.

This result is plagued in the calculation of the QBER for QCKD protocols, such as BB84 and the two variants of the Ekert's protocol, based on either CHSH and Wigner's inequality (Section VI). Previsions about the sifted and the corrected key, the quantum bit error rate before and after a standard error correction procedure are also presented. Furthermore we evaluate the performance of security criteria for Ekert's protocols based on both CHSH inequality and Wigner's inequality (Section VII).

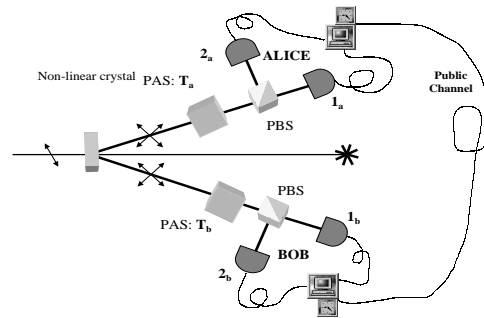


FIG. 1: QCKD set-up: polarization entangled photons generated by SPDC are directed to the two parties (Alice and Bob). The bit sequence of the key is obtained by means of polarization sensitive synchronized measurements performed by Alice and Bob according to a specific QCKD protocol.

II. DECOHERENCE EFFECTS IN PRACTICAL SYSTEMS

The interaction between the quantum system with unobserved "environmental" degrees of freedom and/or measurement system brings about loss of coherence limiting the exploitation of quantum properties in actual quantum information experiments. Even though other groups [27, 28] have already outlined this problem, here we emphasize also some other causes of decoherence by considering different contributions owing to a practical QCKD system.

In Fig. 1 we depict the typical scheme for quantum cryptography key distribution so far implemented by entangled photons, generated by spontaneous parametric down-conversion. Due to a nonlinear interaction in a $\chi^{(2)}$ crystal, some pump photons (angular frequency ω_p) may spontaneously split into lower frequency pair of photons, historically called signal and idler, perfectly correlated in all aspects of their state (direction, energy, polarization, under the constraints of conservation of energy and wavevector momentum, otherwise known as phase-matching). These entangled states show perfect correlation for polarization measurement along orthogonal but arbitrary axes.

The QCKD performed by pure entangled states relies on the realization of two quantum correlated optical channels yielding single-photon polarization states since, whenever Alice performs a polarization measurement on a photon of the pair, automatically the other photon is projected in a defined polarization state, so that we can argue that Alice plays the role of triggering Bob's measurement. Actually the light field emerging from the output of the nonlinear crystal is a polarization entangled multimode state. However it can be described as polarization entangled two-photons state in only two effective modes (one for the a channel and the other for the

channel b), since by using phase-matching rules [29], one can easily produce signal and idler pairs that are emitted non-collinearly with the pump. This scheme eventually is exploited in quantum information applications by using a channel as trigger or reference (a) and the other channel as probe (b). According with Fig. 1 we address the Alice's detection apparatus to the trigger while Bob's to the probe. Alice and Bob detection apparatus are made up by polarization analyzers systems (PAS) allowing proper single beam polarization rotation, polarizing beam splitters (PBS), detectors ($1_a, 2_a, 1_b, 2_b$), storage data systems (computers) and synchronization systems.

Let us consider afterwards the entangled states generated by a type II parametric down-conversion [30], where the output two-photon states result to be a quantum superposition of orthogonally polarized photons in singlet states as [31]

$$|\psi\rangle = \frac{1}{\sqrt{2}} (|H_a\rangle |V_b\rangle - |V_a\rangle |H_b\rangle).$$

Basically here we consider decoherence as the entanglement between the quantum system and the measurement system. In general quantum information experiments, detecting photons means achieving information from the measuring system after the interaction with the quantum system by tracing over specific photon degrees of freedom, like polarization or number of photon pairs. In the following we tie the density matrices $\hat{\rho}_S^{\text{QS}}$ and $\hat{\rho}^{\text{MS}}$, to the quantum system (QS) in a specific state (S) and to the measuring system (MS) before the interaction, respectively, and draw the total input density matrix as

$$\hat{\rho}_S^{\text{in}} = \hat{\rho}_S^{\text{QS}} \otimes \hat{\rho}^{\text{MS}}. \quad (1)$$

By the interaction between QS and MS, represented by the unitary operator $\hat{U}_{\text{QS-MS}}$, we deduce the output density matrix

$$\hat{\rho}_S^{\text{out}} = \hat{U}_{\text{QS-MS}} \hat{\rho}_S^{\text{in}} \hat{U}_{\text{QS-MS}}^\dagger. \quad (2)$$

Finally the measurement outcome yields by tracing over the quantum system degrees of freedom, thus writing the reduced density matrix

$$\hat{\rho}_S^{\text{D}} = \text{Tr}_{\text{QS}}(\hat{\rho}_S^{\text{out}}). \quad (3)$$

Moreover we describe any experimental action projecting the photon density matrix from any particular QS state (S_1) to another state description (S_2) by a unitary transformation $\hat{T} |S_1\rangle = |S_2\rangle$ ruling as

$$\hat{\rho}_{S_2} = \hat{T} \hat{\rho}_{S_1} \hat{T}^\dagger, \quad (4)$$

drawn accordingly to the particular process taken into consideration.

As already mentioned the degrees of freedom of the quantum system considered hereinafter are the entanglement in polarization of photon pairs and the quantum

superposition of photon pair number. These effects are treated separately and then gathered when noise is accounted in MS. Thus with respect to the measurement system we take in consideration firstly the case of a lossless MS and secondly the case of a lossy and noisy one.

In the case of a lossless MS we account for effects due to the imperfect state generation and collection of entangled photons, and to the polarization state selection performed by imperfect polarizing beam splitters (PBSs) together with polarization analyzers (PAs) (see Fig. 1) (Section III.A). Furthermore in Subsection III.B we discuss the effects owing to imperfect collection of uncorrelated photons in lossless detection systems. All decoherence effects on photon density matrix are accounted separately and then summed up according to Eq. (1).

Further decoherence effects are considered when MS is noisy and lossy for it definitely produces a statistical distribution of counted photons. In this respect we examine decoherence due both to the detection system deficiencies inducing losses in counting photon pairs and to the detection system noise and detector dark counts (Subsection IV.A-B).

In Section V we extend the above treated decoherence effects on the coincidence measurements, accounting also for electronic system imperfections associated to non ideal time correlation measurements.

III. DECOHERENCE EFFECTS ON PHOTON PAIRS

In this Section we make allowance for a real non-maximally entangled/partially mixed state generated by SPDC and we analyze the decoherence effects induced by imperfect polarization selection by real PBSs. Furthermore decoherence effects induced on correlated photons by the detection system and by imperfect collection in a lossless measurement system are considered.

A. Polarization selection of photon pairs

In this Subsection we describe the effects of the entanglement between the polarization of photons and a MS leading to decoherence because of imperfect entangled state generation and imperfect selection of polarization state. This analysis yields the reduced density matrix of the outcoming QS subject to these effects.

Practically pure entanglement may not be achieved due to an initial imperfect source generation and afterwards entangled photons collection. Reminding refs. [27, 28] a missed total compensation of a loss of coherence induced in the state by coupling between polarization and frequency modes due to a birefringent environment, may produce residual partially mixed or non-maximally entangled state. On the other hand, more practically, the collection of the same amount of entangled photons on both channels is unlikely mostly for imperfect positioning

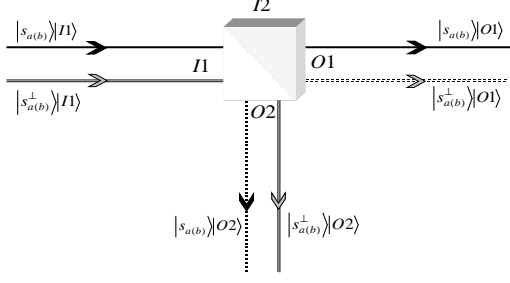


FIG. 2: Real PBS: all photons projected in $|s_{a(b)}^\perp\rangle$ polarized state should be reflected, while some of these are wrongly transmitted. Moreover all photons projected in $|s_{a(b)}\rangle$ polarized state should be transmitted while some of these are erroneously reflected.

of the detection systems with respect to the true position of entangled photons on the SPDC cones. Thus imperfect compensation of dephasing and decoherence in the crystal for non-ideal entangled photon generation together with misalignment in collecting entangled photons in the optical paths are accounted by two complex variables ζ ($|\zeta| \leq 1$) and ϵ , respectively, yielding as a result a non-maximally entangled, or partially mixed state, written as

$$\widehat{\rho}_{\mathcal{L}}^{\psi} = \frac{1}{1 + |\epsilon|^2} \left[|H_a\rangle|V_b\rangle\langle V_b|\langle H_a| + |\epsilon|^2 |V_a\rangle|H_b\rangle\langle H_b|\langle V_a| + \right. \\ \left. - \epsilon\zeta |V_a\rangle|H_b\rangle\langle V_b|\langle H_a| - (\epsilon\zeta)^* |H_a\rangle|V_b\rangle\langle H_b|\langle V_a| \right].$$

We write out the density matrix for the quantum state $\widehat{\rho}_{\mathcal{L}}^{\psi}$ in the base

$$\mathcal{L} : \{|H_a\rangle|H_b\rangle, |V_a\rangle|V_b\rangle, |H_a\rangle|V_b\rangle, |V_a\rangle|H_b\rangle\}.$$

We analyze now the decoherence introduced via the polarization state selection by the MS depicted in Fig. 1: here the entangled photons are detected accordingly to their polarizations by using imperfect polarizing beam splitters (PBSs) on both arms and perfect single photon detectors. The PBSs are considered as part of the MS since they project photons in a polarization base $\mathcal{S} : \{|s_a\rangle|s_b\rangle, |s_a^\perp\rangle|s_b^\perp\rangle, |s_a\rangle|s_b^\perp\rangle, |s_a^\perp\rangle|s_b\rangle\}$, according to the transformations \widehat{T}_a and \widehat{T}_b induced by the polarization analyzer systems (PAs) in each arm ($z = a, b$), defined in this case according to Eq.(4) as

$$\widehat{T}_z |H_z\rangle = |s_z\rangle, \\ \widehat{T}_z |V_z\rangle = |s_z^\perp\rangle.$$

In the case of ideal PBSs in the channel z the state $|s_a\rangle$ ($|s_b\rangle$) is transmitted while the state $|s_a^\perp\rangle$ ($|s_b^\perp\rangle$) is reflected, i.e. there is a perfect entanglement between the

output ports of the PBSs and the projections of the photon polarization state. In the approach so far adopted in literature a perfect entanglement is always assumed since the measurement process is considered as a projection on polarization states $|s_a\rangle, |s_a^\perp\rangle, |s_b\rangle, |s_b^\perp\rangle$, thus assuming detectors $1_a, 1_b, 2_a, 2_b$, sensitive to polarization. Here we consider a further decoherence effect induced by the presence of real PBSs, where a small part of the photons projected in the $|s_a^\perp\rangle$ ($|s_b^\perp\rangle$) are erroneously transmitted, and some photons projected in the state $|s_a\rangle$ ($|s_b\rangle$) are erroneously reflected (generally less than 2% and 5%, respectively), as it is shown in Fig. 2. For this purpose we extend the Hilbert space for describing photon states by accounting also for the paths of photons passing by the input and output ports of the PBSs, thus definitely writing

$$\begin{aligned} |s_z\rangle|O1_z\rangle &= t_z |s_z\rangle|I1_z\rangle + r_z |s_z\rangle|I2_z\rangle \\ |s_z\rangle|O2_z\rangle &= t_z |s_z\rangle|I2_z\rangle + r_z |s_z\rangle|I1_z\rangle \\ |s_z^\perp\rangle|O1_z\rangle &= r_z^\perp |s_z^\perp\rangle|I2_z\rangle + t_z^\perp |s_z^\perp\rangle|I1_z\rangle \\ |s_z^\perp\rangle|O2_z\rangle &= r_z^\perp |s_z^\perp\rangle|I1_z\rangle + t_z^\perp |s_z^\perp\rangle|I2_z\rangle, \end{aligned} \quad (5)$$

where $|Ox_z\rangle$ represent the photons crossing the output ports of the PBS towards detectors x_z and $|Ix_z\rangle$ represent the photon crossing the input port of the PBS, with $x = 1, 2$. $|t_z^\perp|^2$ is the transmittance of photons in the $|s_z^\perp\rangle$ polarization state and $|r_z^\perp|^2 = 1 - |t_z^\perp|^2$ the corresponding reflectance, whose phase relation $r_z^\perp/t_z^\perp = i|r_z^\perp|/|t_z^\perp|$. Analogously $|t_z|^2$ and $|r_z|^2$ are the transmittance and reflectance of photons in the $|s_z\rangle$ state. We spell out that, so far, we have only considered real but lossless PBSs, since the effect of photon losses due to all optical devices used in the channels are postponed to the Section IV.

We therefore define the density matrix for the PBS ports as

$$\widehat{\rho}^{\text{PBS}} = |I1_a\rangle|I1_b\rangle\langle I1_b|\langle I1_a|,$$

and, following the general model of Eq. (1), the total input density matrix of the photon system as

$$\widehat{\rho}_{\mathcal{L}}^{\text{in}} = \widehat{\rho}^{\text{PBS}} \otimes \widehat{\rho}_{\mathcal{L}}^{\psi}.$$

The subscript refers to the space of description of the density matrix. As a further step we consider also the polarization analyzers which independently rule in the corresponding subspaces a and b of the Hilbert space of polarization and induce linear transformation represented by the operators \widehat{T}_a and \widehat{T}_b . Since \widehat{T}_a and \widehat{T}_b are ineffective on the Hilbert space PBS port, $\widehat{\rho}_{\mathcal{L}}^{\text{in}}$ is subject to an overall transformation written as an unitary operator $\widehat{T}_{\mathcal{S}} = \mathbf{1}^{\text{PBS}} \otimes \widehat{T}_{\psi}$ where $\widehat{T}_{\psi} = \widehat{T}_a \otimes \widehat{T}_b$. \widehat{T}_{ψ} induces a basis transformation from \mathcal{L} to \mathcal{S} ($\mathcal{L} \rightarrow \mathcal{S}$).

The new density matrix in the basis \mathcal{S} is thus (Eq. (4))

$$\widehat{\rho}_{\mathcal{S}}^{\text{in}} = \widehat{T}_{\mathcal{S}} \widehat{\rho}_{\mathcal{L}}^{\text{in}} \widehat{T}_{\mathcal{S}}^\dagger = \widehat{\rho}^{\text{PBS}} \otimes \widehat{T}_{\psi} \widehat{\rho}_{\mathcal{L}}^{\psi} \widehat{T}_{\psi}^\dagger. \quad (6)$$

We point out again that in the following \widehat{U} indicates the transformation entangling different Hilbert spaces and \widehat{T} indicates any transformation that changes basis representation. We calculate the output density matrix as in Eq. (2)

$$\widehat{\rho}_S^{\text{out}} = \widehat{U}_{\psi\text{-PBS}} \widehat{\rho}_S^{\text{in}} \widehat{U}_{\psi\text{-PBS}}^\dagger, \quad (7)$$

by applying the unitary transformation $\widehat{U}_{\psi\text{-PBS}}$ describing the entanglement between the photon pair polarization state and the PBS ports, deduced by Eq.s (5). Explicit calculation is reported in Appendix A.

Since the detectors are positioned on the optical paths associated directly to the PBS ports, we deduce the reduced density matrix of the resultant quantum system after the described decoherence processes by tracing over the polarization degrees of freedom according to Eq. (3), obtaining

$$\widehat{\rho}_S^{\text{D}} = \text{Tr}_\psi(\widehat{\rho}_S^{\text{out}}).$$

Thus the probability of detecting the photons pairs by the detectors x_a and y_b is

$$p_S(x_a, y_b) = \langle O x_a | \langle O y_b | \widehat{\rho}_S^{\text{D}} | O y_b \rangle | O x_a \rangle, \quad (8)$$

where $x_a = 1_a, 2_a$, and $y_b = 1_b, 2_b$.

B. Collection of photon pairs

In the following we treat the problem of decoherence on the state "number of photons pairs", induced by an imperfect collection of the correlated photons by the lossless detection system.

Our goal is to determine the resulting density matrix $\widehat{\rho}_\alpha^z$ of the correlated photon pairs detected in each channel $z = a, b$. Therefore the suffix will indicate the QS space of representation and the subscript will refer to the considered quantity, e.g. α stands for the fraction of polarization entangled photon pairs selected by the MS.

In this perspective we define a general density matrix representing the photon pair states in term of photon pair numbers in Alice's and Bob's channels as

$$\widehat{\rho}_\alpha^\gamma = \sum_{n,m=0}^{\infty} \rho_{\alpha,nm}^\gamma |n_a^\gamma\rangle |n_b^\gamma\rangle \langle m_b^\gamma| \langle m_a^\gamma|,$$

and the unitary operators $\widehat{U}_{\gamma-\mu,z}$ acting independently on a and b , whose effect is to entangle the space of the number of photons (γ) with the space of the number of counts (μ) according to

$$\widehat{U}_{\gamma-\mu,z} |n_z^\gamma\rangle |m_z^\mu\rangle = |n_z^\gamma\rangle |(n+m)_z^\mu\rangle.$$

In a lossless MS the density matrix of input counts is $\widehat{\rho}^\mu = |0_a^\mu\rangle |0_b^\mu\rangle \langle 0_b^\mu| \langle 0_a^\mu|$, while the total input density matrix according to Eq. (1) is simply

$$\widehat{\rho}_\alpha^{\text{in}} = \widehat{\rho}_\alpha^\gamma \otimes \widehat{\rho}^\mu,$$

and the output density matrix after the interaction with the detection system results $\widehat{\rho}_\alpha^{\text{out}} = \widehat{U}_{\gamma-\mu,a} \widehat{U}_{\gamma-\mu,b} \widehat{\rho}_\alpha^{\text{in}} \widehat{U}_{\gamma-\mu,b}^\dagger \widehat{U}_{\gamma-\mu,a}^\dagger$.

The reduced density matrix of those photons generated by SPDC and counted by MS exhibits a pure statistical behavior due to the detection process introducing decoherence and reducing the photon pairs counts in a complete mixed state described by the statistical operator according to Eq. (3)

$$\widehat{\rho}_\alpha = \text{Tr}_\gamma(\widehat{\rho}_\alpha^{\text{out}}) = \sum_{n=0}^{\infty} \rho_{\alpha,nn} |n_a\rangle |n_b\rangle \langle n_b| \langle n_a|, \quad (9)$$

where $\rho_{\alpha,nn} = (\lambda_\alpha t)^n \exp(-\lambda_\alpha t)/n!$, being t the time of measurement and λ_α the mean rate of photon pairs in Alice and Bob channels [21, 33, 34, 35]. We explicit now the density matrices ($\widehat{\rho}_\alpha^z$) associated to the photon counts in the single channel z and belonging to correlated pairs (α), by tracing over one of the two channel, as in Eq. (3), respectively

$$\begin{aligned} \widehat{\rho}_\alpha^b &= \text{Tr}_a(\widehat{\rho}_\alpha) = \sum_{n=0}^{\infty} \rho_{\alpha,nn} |n_b\rangle \langle n_b|, \\ \widehat{\rho}_\alpha^a &= \text{Tr}_b(\widehat{\rho}_\alpha) = \sum_{n=0}^{\infty} \rho_{\alpha,nn} |n_a\rangle \langle n_a|. \end{aligned} \quad (10)$$

Experimentally interference filters and diaphragms are properly added to beam splitter polarizers to distinguish the optical paths of entangled photons. These optical elements do not reject unwanted uncorrelated photons due to SPDC itself or additive background photons due to straylight. This happens also in the case of a perfect positioning of the collection system exactly on the entangled photons, and results anyway in an increased degree of uncorrelation, noise fluctuations in coincidence measurements and asymmetry between photons in the two channels, where mean photon rate results to be different.

In this context we evaluate the density matrix $\widehat{\rho}^z$ of total photons counted in the single channel accounting for uncorrelated photon collection, thus we distinguish from the above defined density matrix ($\widehat{\rho}_\alpha^z$) associated to photons belonging to correlated pairs the matrix ($\widehat{\rho}_{1-\alpha}^z$) associated to straylight and uncorrelated photon counts, and write out

$$\widehat{\rho}_{1-\alpha}^z = \sum_{n=0}^{\infty} \rho_{1-\alpha,nn}^z |n_z\rangle \langle n_z|, \quad (11)$$

where $\rho_{1-\alpha,nn}^z = (\lambda_{1-\alpha,z} t)^n \exp(-\lambda_{1-\alpha,z} t)/n!$, being $\lambda_{1-\alpha,z}$ the mean counted photon rate associated to uncorrelated photons. $\widehat{\rho}_{1-\alpha}^z$ is in a completely mixed state for the considerations leading to Eq. (9). The uncorrelated photons present a Poissonian distribution for measurement time $t \gg \lambda_{1-\alpha,z}^{-1}$ [36]. The total density matrix for the single channel is therefore, again applying Eq. (1)

$$\widehat{\rho}_\alpha^z \otimes \widehat{\rho}_{1-\alpha}^z = \sum_{n,m=0}^{\infty} \rho_{1-\alpha,nn}^z \rho_{\alpha,mm} |n_z^{1-\alpha}\rangle |m_z^\alpha\rangle \langle m_z^\alpha| \langle n_z^{1-\alpha}|.$$

By considering the total number of photons counted in the channel z as $l_z = m_z^\alpha + n_z^{1-\alpha}$, we write out $\hat{\rho}_\alpha^z \otimes \hat{\rho}_{1-\alpha}^z = \sum_{m=0}^{\infty} \sum_{l=m}^{\infty} \rho_{1-\alpha, l-m}^z \rho_{\alpha, m}^z |l_z\rangle |m_z^\alpha\rangle \langle m_z^\alpha| \langle l_z|$, where $|l_z\rangle$ univocally substitutes $|n_z^{1-\alpha}\rangle$. The density matrix representing the total number of photons counted in the channel z is obtained tracing over states $|m_z^\alpha\rangle$,

$$\hat{\rho}^z = \sum_{m=0}^{\infty} \langle m_z^\alpha | \hat{\rho}_\alpha^z \otimes \hat{\rho}_{1-\alpha}^z | m_z^\alpha \rangle = \sum_{l=0}^{\infty} \rho_{l l}^z |l_z\rangle \langle l_z|, \quad (12)$$

where $\rho_{l l}^z = \sum_{m=0}^l \rho_{z, l-m}^{1-\alpha} \rho_{l-m}^\alpha = [(\lambda_{1-\alpha, z} + \lambda_\alpha)t]^l \exp[-(\lambda_{1-\alpha, z} + \lambda_\alpha)t]/l!$.

Hereinafter we address λ_z as the mean photon number rate on channel $z = a, b$, being $\alpha_z \lambda_z = \lambda_\alpha$ the mean rate of correlated photons in Alice and Bob channels ($0 < \alpha_z < 1$), and $\lambda_{1-\alpha, z} = (1 - \alpha_z)\lambda_z$ the mean rate of uncorrelated photons, where also the possibility of different levels of correlation is considered by assuming $\alpha_a \neq \alpha_b$. We argue that α_z can be attributed thoroughly to the angular spread of SPDC, thus resulting in a dependence on the inverse squared distance of the source from the detection/collection system, particularly in the open air case rather than in fiber coupling.

IV. DECOHERENCE EFFECTS ON PHOTON COUNTS

For the experimental setup throughout described in Fig. 1, the counted pairs of photons are subjected also to two other actions by the MS: loss mechanisms and noise related to actual detection system.

In the following we calculate the density matrix of total photons counted by any detector x_z ($\hat{\rho}_{\text{tot}}^{x_z}$) by separately addressing a density matrix ($\hat{\rho}^{x_z}$) to photons counted in the presence of detection system deficiencies like non-ideal quantum efficiency, electronics dead time and optical absorbance in the channels, and a density matrix ($\hat{\rho}_d^{x_z}$) associated to the detector dark counts.

A. Detection losses

The next step is to determine the density matrix ($\hat{\rho}^{x_z}$) of single photons randomly counted by x_a or y_b detectors in a lossy system. This process is here described by a unitary transformation \hat{T}_{x_z} , as in Eq. (4), according to

$$\hat{T}_{x_z} |n_z\rangle = \sum_{m=0}^n d_{x_z}(m, n) |m_{x_z}\rangle,$$

by distributing randomly counted photons over any arbitrary detector and considering also loss mechanism through the coefficients $|d_{x_a}(m, n)|^2 = \binom{n}{m} [\xi_{x_a} \sum_{y_b} p_S(x_a, y_b)]^m [1 - \xi_{x_a} \sum_{y_b} p_S(x_a, y_b)]^{n-m}$

and $|d_{y_b}(m, n)|^2 = \binom{n}{m} [\xi_{y_b} \sum_{x_a} p_S(x_a, y_b)]^m [1 - \xi_{y_b} \sum_{x_a} p_S(x_a, y_b)]^{n-m}$. Some other losses due to electronics (π_z) and detection efficiencies (η_{x_z}) as well as optical ones (τ_{x_z}) are summed up by the term $\xi_{x_z} = \pi_z \eta_{x_z} \tau_{x_z}$ [22, 37], while we refer to the Appendix B for the analysis of dead time in this context. We remind that in the term τ_{x_z} we take into consideration any loss in the Alice and Bob optical path, due to crystal, filter, lens, PBSs, PAs and fiber. The terms $\sum_{x_a(y_b)} p_S(x_a, y_b)$ account definitely for the probability that each photon of the pair may be counted randomly by any arbitrary detector.

The density matrix corresponding to correlated photons counted by the detector x_z is obtained by applying the transformation \hat{T}_{x_z} to the density matrix $\hat{\rho}_\alpha^z$ in Eq. (10), as follows

$$\hat{\rho}_\alpha^{x_z} = \hat{T}_{x_z} \hat{\rho}_\alpha^z \hat{T}_{x_z}^\dagger = \sum_{n=m}^{\infty} \sum_{m=0}^{\infty} \rho_{\alpha, n n} |d_{x_z}(m, n)|^2 |m_{x_z}\rangle \langle m_{x_z}|. \quad (13)$$

The $\hat{\rho}_\alpha^{x_a(y_b)}$ diagonal elements are derived accordingly to

$$\rho_{\alpha, m m}^{x_a(y_b)} = [\xi_{x_a(y_b)} \alpha_a \lambda_a t \sum_{y_b(x_a)} p_S(x_a, y_b)]^m / m! \quad (14)$$

$$\exp[-\xi_{x_a(y_b)} \alpha_a \lambda_a t \sum_{y_b(x_a)} p_S(x_a, y_b)].$$

Similarly the density matrix of photon counts due to the straylight on the detector x_z is given by

$$\hat{\rho}_{1-\alpha}^{x_z} = \sum_{n=m}^{\infty} \sum_{m=0}^{\infty} \binom{n}{m} \left(\frac{1}{2}\xi_{x_z}\right)^m \left(1 - \frac{1}{2}\xi_{x_z}\right)^{n-m} \rho_{1-\alpha, n n}^z |m_{x_z}\rangle \langle m_{x_z}|$$

with

$$\rho_{1-\alpha, m m}^{x_z} = [(1 - \alpha_z) \xi_{x_z} \lambda_z t / 2]^m \frac{\exp[-(1 - \alpha_z) \xi_{x_z} \lambda_z t / 2]}{m!}$$

where $\binom{n}{m} (\frac{1}{2}\xi_{x_z})^m (1 - \frac{1}{2}\xi_{x_z})^{n-m}$ is the probability that straylight photons are uniformly distributed over any possible detector.

Analogously to Eq. (12) the density matrix representing the number of photons counted by the generic detector x_z is obtained by tracing over $\hat{\rho}_\alpha^{x_z} \otimes \hat{\rho}_{1-\alpha}^{x_z}$, as

$$\hat{\rho}^{x_z} = \sum_{l=0}^{\infty} \rho_{l l}^{x_z} |l_{x_z}\rangle \langle l_{x_z}|,$$

where $\rho_{l l}^{x_a}$ and $\rho_{l l}^{x_b}$ are Poissonian distributions of the stochastic variable l with mean rates

$$\lambda_{x_a} = \xi_{x_a} \sum_{y_b} p_S(x_a, y_b) \alpha_a \lambda_a t + \frac{1}{2}(1 - \alpha_a) \xi_{x_a} \lambda_a t$$

and

$$\lambda_{x_b} = \xi_{x_b} \sum_{y_a} p_S(y_a, x_b) \alpha_a \lambda_a t + \frac{1}{2} (1 - \alpha_b) \xi_{x_b} \lambda_b t,$$

respectively.

B. Noise

The main noise in detectors is owed to dark counts. Their density matrix is totally statistical and given by $\hat{\rho}_d^{x_z} = \sum_{m=0}^{\infty} \rho_{d,m}^{x_z} |m_{x_z}^d\rangle \langle m_{x_z}^d|$, with diagonal coefficients $\rho_{d,m}^{x_z} = (\lambda_{d,x_z} t)^m \exp(-\lambda_{d,x_z} t) / m!$, being λ_{d,x_z} the mean dark counts. Analogously to Eq. (12) the density matrix representing the total number of counts by the arbitrary detector x_z is obtained by tracing $\hat{\rho}^{x_z} \otimes \hat{\rho}_d^{x_z}$ over states $|m_{x_z}^d\rangle$, yielding

$$\hat{\rho}_{\text{tot}}^{x_z} = \sum_{m=0}^{\infty} \rho_{\text{tot},m}^{x_z} |m_{x_z}\rangle \langle m_{x_z}|,$$

where $\rho_{\text{tot},m}^{x_a}$ and $\rho_{\text{tot},m}^{x_b}$ are Poissonian distributions in the random variable m with mean count rates

$$\begin{aligned} \lambda_{\text{tot},x_a} &= \lambda_{x_a} + \lambda_{d,x_a}, \\ \lambda_{\text{tot},x_b} &= \lambda_{x_b} + \lambda_{d,x_b}, \end{aligned}$$

respectively.

V. DECOHERENCE EFFECTS ON COINCIDENCE COUNTS

One of the main features connected to the use of a faint laser for QCKD consists in a random selection of data performed by Alice rather than by the statistical quantum fluctuations of the entangled states. Even though to some extent in the case of entangled states this point allows a higher degree of randomization, on the other hand the trivial consideration that the triggering (Alice) photon quantum fluctuation enters in the evaluation of the overall noise in the QCKD scheme comes afterward.

From this last argument it ensues the need to build up a model ending up in the density matrix of the total coincidence ($\hat{\rho}_c^{x_a y_b}$), in order to estimate crucial quantities of a typical quantum cryptography key distribution experiment, i.e. the sifted key, the Quantum Bit Error Rate (QBER) before and after the error correction procedure whenever different protocols are applied. For this purpose analogously to Subsection III.B the density matrix $\hat{\rho}_p^{x_a y_b}$ is obtained for pairs counted by a couple of detectors x_a and y_b , while some considerations must be added in order to calculate the density matrix ($\hat{\rho}_{\text{Acc}}^{x_a y_b}$) of accidental coincidences due to imperfections in the detection electronics.

It is straightforward to define a density matrix completely analogous to Eq. (9) in terms of counted pair

states as

$$\hat{\rho}_p = \sum_{n=0}^{\infty} \rho_{\alpha, nn} |n\rangle \langle n|. \quad (15)$$

In order to deduce the density matrix of the coincidences due to the entangled photon pairs counted by the detectors x_a and y_b , indicated by $\hat{\rho}_p^{x_a y_b}$, we observe that a true coincidence count may occur only if both photons of the pair are not lost. Thus analogously to Eq. (13) the density matrix in the Hilbert space of number of counted pairs is

$$\begin{aligned} \hat{\rho}_p^{x_a y_b} &= \hat{T}_{p,x_a y_b} \hat{\rho}_p \hat{T}_{p,x_a y_b}^\dagger = \\ &= \sum_{m=0}^{\infty} \sum_{n=m}^{\infty} \rho_{\alpha, nn} |d_{x_a y_b}(m, n)|^2 |m_{x_a y_b}\rangle \langle m_{x_a y_b}| \end{aligned}$$

where the operator $\hat{T}_{p,x_a y_b}$ induces the transformation $\hat{T}_{p,x_a y_b} |n\rangle = \sum_{m=0}^n d_{x_a y_b}(m, n) |m_{x_a y_b}\rangle$ and the $m_{x_a y_b}$ represents the number of counted pairs that are randomly detected by the couple of detectors x_a and y_b . By $|d_{x_a y_b}(m, n)|^2 = \binom{n}{m} [\xi_{x_a} \xi_{x_b} p_S(x_a, y_b)]^m [1 - \xi_{x_a} \xi_{x_b} p_S(x_a, y_b)]^{n-m}$ we account for the probability $p_S(x_a, y_b)$ that each photon pair definitely may be counted randomly by the couple of x_a and y_b detectors. The $\hat{\rho}_p^{x_a y_b}$ diagonal elements are

$$\rho_{p,mm}^{x_a y_b} = \frac{(\lambda_{p,x_a y_b} t)^m}{m!} \exp(-\lambda_{p,x_a y_b} t),$$

where $\lambda_{p,x_a y_b} = p_S(x_a, y_b) \xi_{x_a} \xi_{y_b} \alpha_a \lambda_a$ is the mean coincidences rate.

Then, a further noise on coincidences to be considered is linked to non ideal time correlation for the presence of a temporal coincidence window $w < D_z$, where D_z is the dead time in the z channel according to Appendix B. This forces to distinguish between true and accidental coincidence statistics. Thus, we deduce the density matrix $\hat{\rho}_{\text{Acc}}^{x_a y_b}$ for accidental coincidences and finally the total density matrix $\hat{\rho}_c^{x_a y_b}$, accounting for true and accidental coincidences.

For accidental counts, we regard the density matrix of the photons counted by the detector x_z possibly yielding accidental coincidences in the time interval Δt , indicated as a noise density matrix, $\hat{\rho}_N^{x_z}$. By observing that matrices $\hat{\rho}_p^{x_a y_b}$ and $\hat{\rho}_{\text{tot}}^{x_z}$ are completely mixed with Poissonian coefficients, it is simple to demonstrate that $\hat{\rho}_N^{x_z} = \sum_{n=0}^{\infty} \rho_{N,nn}^{x_z} |n_{x_z}\rangle \langle n_{x_z}|$, where

$$\begin{aligned} \rho_{N,nn}^{x_a} &= [(\lambda_{\text{tot},x_a} - \sum_{y_b=1_b,2_b} \lambda_{p,x_a y_b}) \Delta t]^n \\ &\quad \frac{\exp[-(\lambda_{\text{tot},x_a} - \sum_{y_b=1_b,2_b} \lambda_{p,x_a y_b}) \Delta t]}{n!}, \\ \rho_{N,nn}^{y_b} &= [(\lambda_{\text{tot},y_b} - \sum_{x_a=1_a,2_a} \lambda_{p,x_a y_b}) \Delta t]^n \\ &\quad \frac{\exp[-(\lambda_{\text{tot},y_b} - \sum_{x_a=1_a,2_a} \lambda_{p,x_a y_b}) \Delta t]}{n!}. \end{aligned}$$

We consider the probability that events revealed by the detectors $y_b = 1_b, 2_b$ occur in coincidence to any event arising from detectors $x_a = 1_a, 2_a$, since the detectors x_a are here considered as the triggering ones. Particularly we distinguish between the contribution of either detectors $y_b = 1_b, 2_b$. Let us indicate by $q_{y_b} = \text{Tr}(\hat{P}_{y_b} \hat{\rho}_N^{y_b})$ the probability that at least a photon on y_b is counted in the coincidence window $\Delta t = w$, where the projector operator $\hat{P}_{y_b} = \sum_{n=1}^{\infty} |n_{y_b}\rangle \langle n_{y_b}|$, thus

$$q_{y_b} = 1 - \exp \left[- \left(\lambda_{\text{tot}, y_b} - \sum_{x_a=1_a, 2_a} \lambda_{p, x_a y_b} \right) w \right]. \quad (16)$$

Since detectors y_b are statistically independent, the probability that both count a photon producing an accidental coincidence is $q_{1_b} q_{2_b}$. The contribution to accidental counts due to detector $1_b(2_b)$ has to be evaluated by considering that the photons may also fall on the other detector $2_b(1_b)$. In this case the overall probability that an event on y_b is counted in the coincidence window w , is obtained from Eq. (16) by subtracting half the probability that both detectors y_b count an accidental photon, thus giving

$$q_{1_b}^* = q_{1_b} \left(1 - \frac{1}{2} q_{2_b} \right), \quad (17)$$

$$q_{2_b}^* = q_{2_b} \left(1 - \frac{1}{2} q_{1_b} \right). \quad (18)$$

The density matrix of accidental coincidence counts $\hat{\rho}_{Acc}^{x_a y_b}$ owing to detectors x_a and y_b can now be deduced by applying the transformation $\hat{T}_{q_{y_b}^*}$ to $\hat{\rho}_N^{x_a}$, the density matrix of those counts triggering possible accidental coincidences in the time measurement $\Delta t = t$, according to $\hat{\rho}_{Acc}^{x_a y_b} = \hat{T}_{q_{y_b}^*} \hat{\rho}_N^{x_a} \hat{T}_{q_{y_b}^*}^\dagger$, where $\hat{T}_{q_{y_b}^*} |n_{x_a}\rangle = \sum_{m=0}^n f_{y_b}(m, n) |m_{x_a y_b}\rangle$, indicating $|f_{y_b}(m, n)|^2 = \binom{n}{m} (q_{y_b}^*)^m (1 - q_{y_b}^*)^{n-m}$, analogously to the Eq. (13). Diagonal elements of $\hat{\rho}_{Acc}^{x_a y_b}$ are Poissonian distributed with mean rate

$$\lambda_{Acc, x_a y_b} = \left(\lambda_{\text{tot}, x_a} - \sum_{y_b=1_b, 2_b} \lambda_{p, x_a y_b} \right) q_{y_b}^*. \quad (19)$$

Lastly the density matrix of total coincidence counts when the presence of the temporal window is accounted for, is indicated by $\hat{\rho}_c^{x_a y_b}$ and as usual by tracing over the true coincidence counts the matrix $\hat{\rho}_p^{x_a y_b} \otimes \hat{\rho}_{Acc}^{x_a y_b}$, following again Eq. (12), we obtain a completely statistical density matrix whose diagonal coefficients are

$$\rho_{c, mm}^{x_a y_b} = (\lambda_{c, x_a y_b} t)^m / m! \exp(-\lambda_{c, x_a y_b} t).$$

The mean rate of total coincidence measured by arbitrary x_a and y_b detectors is

$$\lambda_{c, x_a y_b} = \lambda_{p, x_a y_b} + \lambda_{Acc, x_a y_b}. \quad (20)$$

To characterize a particular QCKD procedure we embody the transformations \hat{T}_a and \hat{T}_b accordingly to the above mentioned QCKD procedure measurement and represent a particular analyzer action on photon polarization by the rotation matrices

$$\hat{T}_z = \begin{pmatrix} \cos \theta_z & \sin \theta_z \\ \sin \theta_z & -\cos \theta_z \end{pmatrix}. \quad (21)$$

In this case Eq. (8) is rewritten in terms of the rotation angles with $p_S(x_a, y_b) \rightarrow p_{\theta_a, \theta_b}(x_a, y_b)$, whose complete expression is in the Appendix A.

More specifically the total coincidence density matrix is explicit in terms of angular settings θ_a and θ_b , as

$$\rho_{c, mm}^{x_a y_b}(\theta_a, \theta_b) = [\lambda_{c, x_a y_b}(\theta_a, \theta_b) t]^m \exp[-\lambda_{c, x_a y_b}(\theta_a, \theta_b) t] / m!,$$

where the measured coincident counts are therefore

$$\lambda_{c, x_a y_b}(\theta_a, \theta_b) t = \text{Tr}\{\hat{n} \hat{\rho}_c^{x_a y_b}(\theta_a, \theta_b)\}.$$

VI. EVALUATION OF QBER

In order to characterize a particular QCKD procedure and to assess its advantages, we evaluate peculiar quantities such as the Quantum Bit Error Rate (QBER) and the sifted key for different types of QCKD protocols so far experimentally implemented, i.e. BB84 protocol and Ekert's protocol based on CHSH and Wigner's inequality, respectively.

The QBER is a parameter for describing the signal quality in the transmission of the sifted key, defined as the relative frequency of errors, i.e. the number of errors divided by the total size of the cryptographic sifted key (K) [35].

A. BB84 protocol

Here we examine as an instance the BB84 protocol variant proposed for entangled states in ref. [3]. We just remind that Alice and Bob measure photons randomly and independently between two bases of orthogonal quantum states. One basis corresponds to horizontal and vertical linear polarization (\oplus), while the other to linear polarizations rotated by 45° (\otimes). As only the subset of measurements performed with the two analyzers in the same basis contributes to the sifted key, while the other subset is discarded, thus only half of the photon pairs can contribute.

The sifted key is given by

$$K_{\text{BB84}}(\theta_a) = f_{\text{basis}} f_{\text{setting}} \sum_{x_a y_b} \left[\lambda_{c, x_a y_b}(\theta_a, \theta_a) + \lambda_{c, x_a y_b}(\theta_a + \pi/4, \theta_a + \pi/4) \right] t, \quad (22)$$

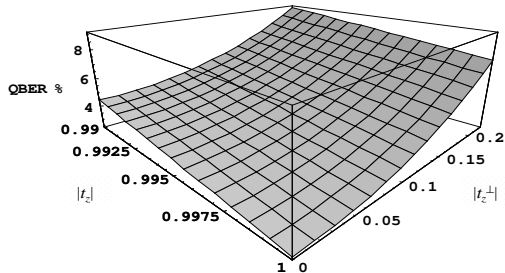


FIG. 3: QBER for the BB84 protocol versus the PBS's coefficients $|t_z|$ and $|t_z^\perp|$.

where $f_{basis} = 1/2$ is the probability to measure in the right basis ((θ_a, θ_a) and $(\theta_a + \pi/4, \theta_a + \pi/4)$), while $f_{setting} = 1/2$ is the probability to measure in a particular analyzers setting ((θ_a, θ_a) or $(\theta_a + \pi/4, \theta_a + \pi/4)$).

All the detectors contribute to the sifted key K but $1_a 2_b$ and $2_a 1_b$ contribute to the true coincidences when measurements are performed in the same basis ($\theta_a = \theta_b$), while QBER contributions come from the coincidences between detectors $1_a 1_b$ and $2_a 2_b$ (as it is clear from Eq.s (A1) in Appendix A). Therefore the $\text{QBER}_{\text{BB84}}$ explicit formula is

$$\text{QBER}_{\text{BB84}}(\theta_a) = \frac{\sum_{x=1,2} \left[\frac{\lambda_{c,x_a x_b}(\theta_a, \theta_a) + \lambda_{c,x_a x_b}(\theta_a + \pi/4, \theta_a + \pi/4)}{4K_{\text{BB84}}(\theta_a)} \right] t}{(23)}$$

To test the influence of decoherence on QBER, we simulate a realistic experiment where parameters are set as $\eta_{x_a} = \eta_{y_b} = 0.5$ (quantum efficiency of the four detectors), $\tau_{x_a} = \tau_{y_b} = 0.1$ (transmittance of the four channels), $\lambda_{d,x_a} = \lambda_{d,y_b} = 50 \text{ s}^{-1}$ (dark count rate of the four detector), $D_a = D_b = 100 \text{ ns}$ (total dead time of the Alice's and Bob detection systems), $\theta_a = 0$ and $w = 4 \text{ ns}$. The entanglement parameters are set according to $\epsilon = 0.95$ and $\zeta = 1$; and the correlation level in the Alice channel $\alpha_a = 0.25$ and the correlated photons $\alpha_a \lambda_a = 700 \text{ KHz}$.

In Fig. 3 we report the dependence of QBER versus the optical properties of actual PBS, i.e. the transmittance $|t_z|$ and $|t_z^\perp|$ ($z = a, b$) for the states $|s_z\rangle$ and $|s_z^\perp\rangle$ respectively.

In Fig. 4 the behavior of the QBER is presented versus α_a the level of correlation in the Alice channel and $\alpha_a \lambda_a$ the rate of the correlated photon pairs for two different noise levels represented by λ_b/λ_a the ratio between the mean rate of photon on the two channels. Note that far from the ideal condition the presence of uncorrelated events in the two channels induce a non-linear increasing of the QBER. The other parameters are set as in Fig.

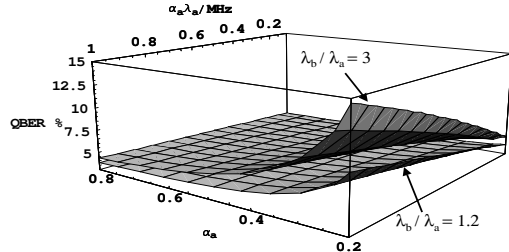


FIG. 4: QBER for the BB84 protocol, the QBER is presented versus the correlation level in the Alice channel α_a and the correlated photons $\alpha_a \lambda_a$ for two noise levels in the channels ($\lambda_b/\lambda_a = 1.2$ and 3).

3 for realistic PBSs parameters set as $|t_z|^2 = 0.99$ and $|t_z^\perp|^2 = 0.025$.

B. Ekert's protocol

Any Ekert's protocol has the peculiarity to rely its security on the completeness of quantum mechanics. Therefore the possible combined choices between Alice and Bob for analyzer settings splits out in three groups: the first for key distribution, the second containing the security proof and the third garnering the discarded measurements.

We here consider two possible variants of Ekert's protocol: variant of Ekert's protocol based on the Clauser-Horne-Shimony-Holt inequality (CHSH) similar to the one proposed in ref. [8] and Ekert's protocol based on Wigner's inequality [7].

1. Ekert's protocol based on Bell's inequality

In order to increase the number of measurements devoted to the key distribution we consider the case where Alice and Bob measure randomly among four analyzer settings and use CHSH inequality to test eavesdropping. In this scheme Alice's choices for the analyzer settings are identified by $\theta_a = (\theta_a, \theta_a + \pi/8, \theta_a + \pi/4, \theta_a + 3\pi/8)$ and Bob's are $\theta_b = (\theta_a + \pi/8, \theta_a + \pi/4, \theta_a + 3\pi/8, \theta_a + \pi/2)$, accordingly.

The key distribution is performed when Alice and Bob settings are the same or orthogonal, so that the sifted

key results

$$K_{\text{CHSH}}(\theta_a) = f_{\text{setting}} \sum_{x_a y_b} \left[\begin{array}{l} \lambda_{c,x_a y_b}(\theta_a, \theta_a + \pi/2) + \\ \lambda_{c,x_a y_b}(\theta_a + \pi/8, \theta_a + \pi/8) + \\ \lambda_{c,x_a y_b}(\theta_a + \pi/4, \theta_a + \pi/4) + \\ \lambda_{c,x_a y_b}(\theta_a + 3\pi/8, \theta_a + 3\pi/8) \end{array} \right] t,$$

where $((\theta_a, \theta_a + \pi/2), (\theta_a + \pi/8, \theta_a + \pi/8), (\theta_a + \pi/4, \theta_a +$

$\pi/4), (\theta_a + 3\pi/8, \theta_a + 3\pi/8))$ are angular settings generating the key and $f_{\text{setting}} = 1/16$.

In a maximally entangled state configuration the detectors contributing to the key should be $1_a 1_b$ and $2_a 2_b$ for the orthogonal analyzer settings while $1_a 2_b$ and $2_a 1_b$ for the parallel settings. Thus the QBER is calculated according to

$$\text{QBER}_{\text{CHSH}}(\theta_a) = \frac{1}{4K_{\text{CHSH}}(\theta_a)} \left\{ \sum_{x_a = y_b} \left[\lambda_{c,x_a y_b}(\theta_a + \pi/8, \theta_a + \pi/8) + \lambda_{c,x_a y_b}(\theta_a + \pi/4, \theta_a + \pi/4) + \lambda_{c,x_a y_b}(\theta_a + 3\pi/8, \theta_a + 3\pi/8) \right] t + \sum_{x_a \neq y_b} \lambda_{c,x_a y_b}(\theta_a, \theta_a + \pi/2) t \right\},$$

where we indicate by the intuitive formalism as $\sum_{x_a \neq y_b}$ the sum over $1_a 2_b$ and $2_a 1_b$ detectors, while with $\sum_{x_a = y_b}$ the sum over $1_a 1_b$ and $2_a 2_b$.

2. Ekert's protocol based on Wigner's inequality

As in ref. [7] we consider the case of the Ekert's variant where the security of the quantum channels is pursued by Wigner's inequality. In this case Alice and Bob measure randomly among four analyzers' settings whose choices are respectively $\theta_a = (\theta_a - \pi/6, \theta_a)$ and Bob's are accordingly $\theta_b = (\theta_a, \theta_a + \pi/6)$.

The key distribution is performed when Alice and Bob settings are the same so that the sifted key results

$$K_{\text{WI}}(\theta_a) = f_{\text{setting}} \sum_{x_a y_b} \lambda_{c,x_a y_b}(\theta_a, \theta_a) t,$$

for $f_{\text{setting}} = 1/4$.

The QBER is calculated according to

$$\text{QBER}_{\text{WI}}(\theta_a) = f_{\text{setting}} \frac{[\lambda_{c,1_a 1_b}(\theta_a, \theta_a) + \lambda_{c,2_a 2_b}(\theta_a, \theta_a)] t}{K_{\text{WI}}(\theta_a)},$$

by considering that detectors contributing to the wrong bits are $1_a 1_b$ and $2_a 2_b$.

In Fig. 5 we present a comparison of QBER levels versus the analyzers angular setting θ_a and the entanglement parameter ϵ in the same (low noise) experimental condition of Figs 3 and 4 for the BB84 protocol and the Ekert protocols considering both the case of CHSH and Wigner's inequality. We highlight that the QBER is sensitive to the angle θ_a in both the cases of the Ekert's protocol based on CHSH and Wigner's inequality, even though stronger in the latter case, leading to the consideration that the Ekert's protocol based on Wigner's inequality can be considered less robust with respect to BB84 and the CHSH based Ekert's protocol.

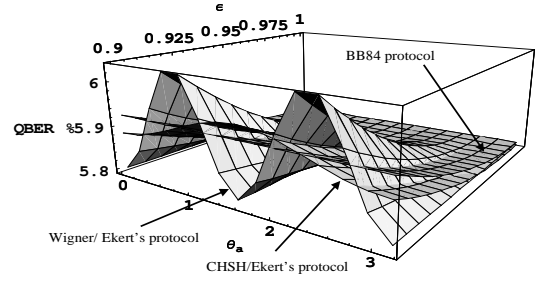


FIG. 5: QBER in the case of CHSH and Wigner's inequality based Ekert's protocols together with BB84 protocol versus the angular analyzers settings θ_a and the entanglement parameter ϵ . The parameters settings are $\lambda_a = 2.8 \cdot 10^6 \text{ s}^{-1}$, $\alpha_a = 0.25$, $\lambda_b/\lambda_a = 1.2$, $\eta_{x_a} = \eta_{y_b} = 0.5$, $\tau_{x_a} = \tau_{y_b} = 0.1$, $\lambda_{d,x_a} = \lambda_{d,y_b} = 50 \text{ s}^{-1}$, $D_a = D_b = 100 \text{ ns}$, $w = 4 \text{ ns}$ and $\zeta = 1$, taken from typical and experimental realistic values so far implemented in literature. PBSs are considered real with $|t_z|^2 = 0.99$ and $|t_z^\perp|^2 = 0.025$ ($z = a, b$).

VII. SECURITY AND ERROR CORRECTION

The security of BB84 variant protocol is based on a public comparison between Alice and Bob's measurements on a sufficiently large random subset of the sifted key, e.g. more than half is recommended in [3].

For practical motivations we introduce the normalized coincidence rate as being function of the analyzer settings and detectors choices accordingly

$$M_{x_a y_b}(\theta_a, \theta_b) = \frac{\lambda_{c,x_a y_b}(\theta_a, \theta_b)}{\sum_{x_a y_b} \lambda_{c,x_a y_b}(\theta_a, \theta_b)}.$$

The terms $M_{x_a y_b}(\theta_a, \theta_b)$ are commonly stored when experiments are performed.

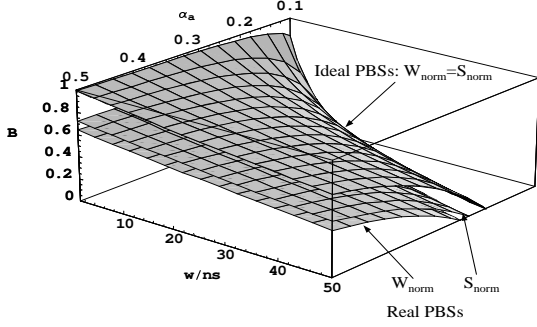


FIG. 6: The CHSH and Wigner's inequalities parameter B versus the coincidence window w and the correlation level in the Alice channel α_a . In the case of maximally entangled states $B = 1$, while the lower cut is defined by the eavesdropping limit $B \leq 0$. The parameter B represents either $S_{\text{norm}} = (|S| - |S_{\text{eve}}|) / (|S_{\text{ql}}| - |S_{\text{eve}}|)$ or $W_{\text{norm}} = (W - W_{\text{eve}}) / (W_{\text{ql}} - W_{\text{eve}})$. The choice of parameter values are the same of Fig. 4 except for $\theta_a = 0$ and $\epsilon = 0.95$. The lower two surfaces represented correspond to W_{norm} and S_{norm} in the case of real PBSs, this latter with parameters $|t_z|^2 = 0.98$ and $|t_z^\perp|^2 = 0.05$. The higher surface represents $S_{\text{norm}} = W_{\text{norm}}$ in the case of ideal PBSs.

The security proof for the CHSH inequality based Ekert's protocol is evaluated with the actual choices of settings by the CHSH inequality

$$\begin{aligned}
 S(\theta_a) &= E(\theta_a, \theta_a + \pi/8) - E(\theta_a, \theta_a + 3\pi/8) + \\
 &\quad E(\theta_a + \pi/4, \theta_a + \pi/8) + E(\theta_a + \pi/4, \theta_a + 3\pi/8), \\
 S'(\theta_a) &= E(\theta_a + \pi/8, \theta_a + \pi/4) - E(\theta_a + \pi/8, \theta_a + \pi/2) + \\
 &\quad E(\theta_a + 3\pi/8, \theta_a + \pi/4) + E(\theta_a + 3\pi/8, \theta_a + \pi/2),
 \end{aligned}$$

where

$$\begin{aligned}
 E(\theta_a, \theta_b) &= M_{1_a 1_b}(\theta_a, \theta_b) - M_{1_a 2_b}(\theta_a, \theta_b) + \\
 &\quad M_{2_a 2_b}(\theta_a, \theta_b) - M_{2_a 1_b}(\theta_a, \theta_b).
 \end{aligned}$$

We remind that for the maximally entangled states $|S_{\text{ql}}| = |S'_{\text{ql}}| = 2\sqrt{2}$ while for any realistic local theory gives as a result $|S, S'| \leq 2$. However it is expected that the presence of an eavesdropper will reduce the observed value of $|S, S'|$, giving $|S_{\text{eve}}, S'_{\text{eve}}| \leq \sqrt{2}$, when the eavesdropper measures photons over either one or both (total eavesdropping) Alice's and Bob's channels [2].

While in the case of Wigner's inequality based Ekert's protocol the Wigner's inequality result

$$\begin{aligned}
 W(\theta_a) &= M_{1_a 1_b}(\theta_a - \pi/6, \theta_a) + M_{1_a 1_b}(\theta_a, \theta_a + \pi/6) + \\
 &\quad - M_{1_a 1_b}(\theta_a - \pi/6, \theta_a + \pi/6),
 \end{aligned}$$

whose outcome for the maximally entangled states is $W_{\text{ql}} = -1/8$ while any local realistic theory gives $W \geq 0$. As for CHSH inequality we proved in Appendix C that

in the case Eve detects only one photon of the pair the limit for W is higher, $W_{\text{eve}} \geq 1/16$, while in the case of total eavesdropping there is no boundary condition.

Protocol based on Wigner's inequality can be considered less robust than a CHSH inequality based one for Wigner's security test guarantees against eavesdropping strategies limited to one photon of the pair detection while CHSH security is independent on the adopted strategy (see Appendix C and ref. [2]). Furthermore, even in the case of single channel eavesdropping attack, the weakness of Wigner's test is coming out in Fig. 6, by comparing behaviors of the CHSH and Wigner's inequality parameters, $S_{\text{norm}} = (|S| - |S_{\text{eve}}|) / (|S_{\text{ql}}| - |S_{\text{eve}}|)$ and $W_{\text{norm}} = (W - W_{\text{eve}}) / (W_{\text{ql}} - W_{\text{eve}})$, respectively, versus the coincidence window w and the correlation level in the Alice's channel, α_a . The lower surfaces represent the case of real PBSs where $W_{\text{norm}} < S_{\text{norm}}$, while the higher surface corresponds to ideal PBSs where $W_{\text{norm}} = S_{\text{norm}}$. We observe that, provided the same system noise level and real PBSs, Wigner's parameter reaches faster than CHSH one the eavesdropping limit.

A satisfactory protocol must be able to recover from noise as well as partial leakage allowing Alice and Bob to reconcile the two string of bits measured and distill from the sifted key a corrected key. We remind that a strong request for the application of any error correction method is an a priori knowledge of the QBER, that provides the information of how many times the error correction procedure must be applied in order to reduce QBER under a certain agreed level, commonly 1%. Here we show an example of error correction on an a priori evaluated QBER according to a common approach reported also in ref. [7], in order to show that this model allow a prevision of the corrected key length.

It's important to highlight that Alice and Bob, in general, cannot distinguish between errors caused either by an eavesdropper or by the environment, thus to rely on the key generated they have to assume that all errors are due to an eavesdropper and evaluate the leaked information from the QBER. We lastly make allowance that even though by the error correction procedure one can disregard wrong bits by simple dropping them in building the distilled key, actually the residual knowledge of an eavesdropper may not be faithfully quantified by the reduced QBER obtained after the correction. This may be easily explained by considering that the effects of Eve's strategy is equivalent to introduce quantum noise yielding eventually accidental coincidence, these last contributing both to wrong and right bits transmitted, as it is clear from the Eq.s (22, 23). This means that the error correction procedure is not suitable to cancel possible Eve's knowledge of the part of the key due to accidental coincidence.

To prove this last assertion we show how error correction procedure is not able to reduce at the QBER level the quantum accidental bit rate (QABR). We explicit the QABR as an example in the case of Ekert's protocol

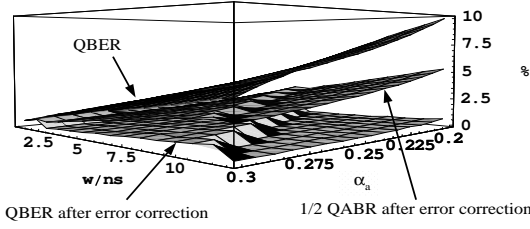


FIG. 7: The CHSH and Wigner’s inequalities parameter B versus the coincidence window w and the correlation level in the Alice channel α_a . In the case of maximally entangled states $B = 1$, while the lower cut is defined by the eavesdropping limit $B \leq 0$. The parameter B represents either $S_{\text{norm}} = (|S| - |S_{\text{eve}}|) / (|S_{\text{ql}}| - |S_{\text{eve}}|)$ or $W_{\text{norm}} = (W - W_{\text{eve}}) / (W_{\text{ql}} - W_{\text{eve}})$. The choice of parameter values are the same of Fig. 4 except for $\theta_a = 0$ and $\epsilon = 0.95$. The lower two surfaces represented correspond to W_{norm} and S_{norm} in the case of real PBSs, this latter with parameters $|t_z|^2 = 0.98$ and $|t_z^\perp|^2 = 0.05$. The higher surface represents $S_{\text{norm}} = W_{\text{norm}}$ in the case of ideal PBSs.

based on Wigner’s inequality

$$\text{QABR}_{\text{WI}}(\theta_a) = f_{\text{setting}} \frac{\sum_{x_a y_b} \lambda_{\text{Acc}, x_a y_b}(\theta_a, \theta_a) t}{K_{\text{WI}}(\theta_a)},$$

In Fig. 7 we present the QBER with and without the application of the error correction procedure together with the 1/2 QABR for the Ekert’s protocol based on Wigner’s inequality versus the coincidence window and the correlation parameter in the Alice channel. We highlight that the error correction procedure is not able to cancel out completely the rising of the QABR as well as the possible Eve’s knowledge on the corrected key.

VIII. CONCLUSIONS

This paper concerns with an a priori evaluation of QCKD crucial parameters when entangled photons produced by SPDC are exploited as quantum system in QCKD practical realization, whose basic experimental peculiarity belongs to the detection of coincident photons. To this aim we developed a statistical model to calculate the density matrix of accidental coincidences for these last specifically might contribute to errors in the sifted key, otherwise not completely accounted for by simple experimental means. This model treats the out-

coming statistical noise in QCKD system as a residual effect of decoherence due to the entanglement between the two-photons quantum system degrees of freedom, such as polarization and number of photon pairs, with the environment and the measurement system.

We dedicated a relevant theoretical part to those decoherence features associated to imperfect source generation and selection, to polarization states analysis performed by imperfect polarizing beam splitters, to photon number detection, to noisy and lossy measurement system. We emphasized basically system imperfections owing to uncorrelated photons collection, detection system deficiencies, detection system noise due to detectors dark counts, as well as electronic system imperfections associated to non ideal time correlation measurements.

We discussed how this model can be adopted for the evaluation of the Quantum Bit Error Rate and the sifted key for different well known protocols, BB84 and Ekert’s protocol based on both CHSH and Wigner’s inequality, comparing them to expected results.

Given that this model predicts precisely the quantum bit error rate and the sifted key, it ultimately guarantees a method to compare different security criteria of the hitherto proposed QCKD protocols and provides an objective assessment of performances and advantages of different systems, thus yielding a method for an a priori evaluation of the tolerable experimental imperfections in a practically implemented quantum system to establish the degree of security and competitiveness of QCKD systems.

Eventually we plugged in the model to a standard error correction procedure observing that this last does not completely cancel the possible residual eavesdropping knowledge on the corrected key, thus we emphasize that this model yields also the degree of security of the corrected key, if a precise modeling and measurement of system imperfections is provided. We lastly argue that a challenging goal in the field of QKCD is a precise quantification of entanglement parameters, i.e. a punctual tomography of the input two-photon state.

APPENDIX A: DECOHERENCE INTERACTION MATRIX $\hat{U}_{\psi\text{-PBS}}$

We explicitly calculate the unitary transformation $\hat{U}_{\psi\text{-PBS}}$ according to Eq.s (5) obtaining a 16×16 matrix

$$\hat{U}_{\psi\text{-PBS}} = \begin{pmatrix} U_1 & U_2 & U_3 & U_4 \\ U_2 & U_1 & U_4 & U_3 \\ U_3 & U_4 & U_1 & U_2 \\ U_4 & U_3 & U_2 & U_1 \end{pmatrix},$$

where we indicate

$$\begin{aligned}
U_1 &= \begin{bmatrix} \mathcal{T}_a \mathcal{T}_b & 0 & 0 & 0 \\ 0 & \mathcal{T}_a \mathcal{T}_b^\perp & 0 & 0 \\ 0 & 0 & \mathcal{T}_a^\perp \mathcal{T}_b & 0 \\ 0 & 0 & 0 & \mathcal{T}_a^\perp \mathcal{T}_b^\perp \end{bmatrix}; & U_2 &= \begin{bmatrix} \mathcal{T}_a \mathcal{R}_b & 0 & 0 & 0 \\ 0 & \mathcal{T}_a \mathcal{R}_b^\perp & 0 & 0 \\ 0 & 0 & \mathcal{T}_a^\perp \mathcal{R}_b & 0 \\ 0 & 0 & 0 & \mathcal{T}_a^\perp \mathcal{R}_b^\perp \end{bmatrix} \\
U_3 &= \begin{bmatrix} \mathcal{R}_a \mathcal{T}_b & 0 & 0 & 0 \\ 0 & \mathcal{R}_a \mathcal{T}_b^\perp & 0 & 0 \\ 0 & 0 & \mathcal{R}_a^\perp \mathcal{T}_b & 0 \\ 0 & 0 & 0 & \mathcal{R}_a^\perp \mathcal{T}_b^\perp \end{bmatrix}; & U_4 &= \begin{bmatrix} \mathcal{R}_a \mathcal{R}_b & 0 & 0 & 0 \\ 0 & \mathcal{R}_a \mathcal{R}_b^\perp & 0 & 0 \\ 0 & 0 & \mathcal{R}_a^\perp \mathcal{R}_b & 0 \\ 0 & 0 & 0 & \mathcal{R}_a^\perp \mathcal{R}_b^\perp \end{bmatrix}
\end{aligned}$$

and $\mathcal{T}_z = t_z/(t_z^2 - r_z^2)$, $\mathcal{R}_z = r_z/(t_z^2 - r_z^2)$ ($z = a, b$), analogously for \mathcal{T}_z^\perp and \mathcal{R}_z^\perp .

According with Eq.s (6), (7) and (21) we obtain for $p_{\theta_a, \theta_b}(x_a, y_b)$ the following

$$\begin{aligned}
p_{\theta_a, \theta_b}(1_a, 1_b) &= \frac{1}{1 + |\epsilon|^2} \left\{ \begin{aligned} &\cos^2(\theta_b) \left[\cos^2(\theta_a) \left(|\mathcal{T}_a \mathcal{T}_b^\perp|^2 + |\mathcal{T}_a^\perp \mathcal{T}_b \epsilon|^2 \right) + \sin^2(\theta_a) \left(|\mathcal{T}_a^\perp \mathcal{T}_b^\perp|^2 + |\mathcal{T}_a \mathcal{T}_b \epsilon|^2 \right) \right] + \\ &\sin^2(\theta_b) \left[\cos^2(\theta_a) \left(|\mathcal{T}_a \mathcal{T}_b|^2 + |\mathcal{T}_a^\perp \mathcal{T}_b^\perp \epsilon|^2 \right) + \sin^2(\theta_a) \left(|\mathcal{T}_a^\perp \mathcal{T}_b|^2 + |\mathcal{T}_a \mathcal{T}_b^\perp \epsilon|^2 \right) \right] + \\ &\sin(2\theta_a) \cos(2\theta_b) \text{Re}(\epsilon \zeta / 2) \left(-|\mathcal{T}_a \mathcal{T}_b|^2 + |\mathcal{T}_a^\perp \mathcal{T}_b|^2 + |\mathcal{T}_a \mathcal{T}_b^\perp|^2 - |\mathcal{T}_a^\perp \mathcal{T}_b^\perp|^2 \right) \end{aligned} \right\}, \\
p_{\theta_a, \theta_b}(1_a, 2_b) &= \frac{1}{1 + |\epsilon|^2} \left\{ \begin{aligned} &\cos^2(\theta_b) \left[\cos^2(\theta_a) \left(|\mathcal{T}_a \mathcal{R}_b^\perp|^2 + |\mathcal{T}_a^\perp \mathcal{R}_b \epsilon|^2 \right) + \sin^2(\theta_a) \left(|\mathcal{T}_a^\perp \mathcal{R}_b^\perp|^2 + |\mathcal{T}_a \mathcal{R}_b \epsilon|^2 \right) \right] + \\ &\sin^2(\theta_b) \left[\cos^2(\theta_a) \left(|\mathcal{T}_a \mathcal{R}_b|^2 + |\mathcal{T}_a^\perp \mathcal{R}_b^\perp \epsilon|^2 \right) + \sin^2(\theta_a) \left(|\mathcal{T}_a^\perp \mathcal{R}_b|^2 + |\mathcal{T}_a \mathcal{R}_b^\perp \epsilon|^2 \right) \right] + \\ &\sin(2\theta_a) \cos(2\theta_b) \text{Re}(\epsilon \zeta / 2) \left(-|\mathcal{T}_a \mathcal{R}_b|^2 + |\mathcal{T}_a^\perp \mathcal{R}_b|^2 + |\mathcal{T}_a \mathcal{R}_b^\perp|^2 - |\mathcal{T}_a^\perp \mathcal{R}_b^\perp|^2 \right) \end{aligned} \right\}, \\
p_{\theta_a, \theta_b}(2_a, 1_b) &= \frac{1}{1 + |\epsilon|^2} \left\{ \begin{aligned} &\cos^2(\theta_b) \left[\cos^2(\theta_a) \left(|\mathcal{R}_a \mathcal{T}_b^\perp|^2 + |\mathcal{R}_a^\perp \mathcal{T}_b \epsilon|^2 \right) + \sin^2(\theta_a) \left(|\mathcal{R}_a^\perp \mathcal{T}_b^\perp|^2 + |\mathcal{R}_a \mathcal{T}_b \epsilon|^2 \right) \right] + \\ &\sin^2(\theta_b) \left[\cos^2(\theta_a) \left(|\mathcal{R}_a \mathcal{T}_b|^2 + |\mathcal{R}_a^\perp \mathcal{T}_b^\perp \epsilon|^2 \right) + \sin^2(\theta_a) \left(|\mathcal{R}_a^\perp \mathcal{T}_b|^2 + |\mathcal{R}_a \mathcal{T}_b^\perp \epsilon|^2 \right) \right] + \\ &\sin(2\theta_a) \cos(2\theta_b) \text{Re}(\epsilon \zeta / 2) \left(-|\mathcal{R}_a \mathcal{T}_b|^2 + |\mathcal{R}_a^\perp \mathcal{T}_b|^2 + |\mathcal{R}_a \mathcal{T}_b^\perp|^2 - |\mathcal{R}_a^\perp \mathcal{T}_b^\perp|^2 \right) \end{aligned} \right\}, \\
p_{\theta_a, \theta_b}(2_a, 2_b) &= \frac{1}{1 + |\epsilon|^2} \left\{ \begin{aligned} &\cos^2(\theta_b) \left[\cos^2(\theta_a) \left(|\mathcal{R}_a \mathcal{R}_b^\perp|^2 + |\mathcal{R}_a^\perp \mathcal{R}_b \epsilon|^2 \right) + \sin^2(\theta_a) \left(|\mathcal{R}_a^\perp \mathcal{R}_b^\perp|^2 + |\mathcal{R}_a \mathcal{R}_b \epsilon|^2 \right) \right] + \\ &\sin^2(\theta_b) \left[\cos^2(\theta_a) \left(|\mathcal{R}_a \mathcal{R}_b|^2 + |\mathcal{R}_a^\perp \mathcal{R}_b^\perp \epsilon|^2 \right) + \sin^2(\theta_a) \left(|\mathcal{R}_a^\perp \mathcal{R}_b|^2 + |\mathcal{R}_a \mathcal{R}_b^\perp \epsilon|^2 \right) \right] + \\ &\sin(2\theta_a) \cos(2\theta_b) \text{Re}(\epsilon \zeta / 2) \left(-|\mathcal{R}_a \mathcal{R}_b|^2 + |\mathcal{R}_a^\perp \mathcal{R}_b|^2 + |\mathcal{R}_a \mathcal{R}_b^\perp|^2 - |\mathcal{R}_a^\perp \mathcal{R}_b^\perp|^2 \right) \end{aligned} \right\}.
\end{aligned}$$

In the case of maximally entangled states, i.e. $\epsilon = 1$ and $\zeta = 1$, and ideal PBSs, i.e. $|\mathcal{R}_z| = |\mathcal{T}_z^\perp| = 0$ and $|\mathcal{R}_z^\perp| = |\mathcal{T}_z| = 1$, the $\hat{U}_{\psi\text{-PBS}}$ is simply given by

$$\begin{aligned}
U_1 &= \begin{bmatrix} 1 & 0 & 0 & 0 \\ 0 & 0 & 0 & 0 \\ 0 & 0 & 0 & 0 \\ 0 & 0 & 0 & 0 \end{bmatrix}; & U_2 &= \begin{bmatrix} 0 & 0 & 0 & 0 \\ 0 & i & 0 & 0 \\ 0 & 0 & 0 & 0 \\ 0 & 0 & 0 & 0 \end{bmatrix} \\
U_3 &= \begin{bmatrix} 0 & 0 & 0 & 0 \\ 0 & 0 & 0 & 0 \\ 0 & 0 & i & 0 \\ 0 & 0 & 0 & 0 \end{bmatrix}; & U_4 &= \begin{bmatrix} 0 & 0 & 0 & 0 \\ 0 & 0 & 0 & 0 \\ 0 & 0 & 0 & 0 \\ 0 & 0 & 0 & 1 \end{bmatrix}
\end{aligned}$$

and

$$\begin{aligned}
p_{\theta_a, \theta_b}(1_a, 1_b) &= p_{\theta_a, \theta_b}(2_a, 2_b) = \sin^2(\theta_a - \theta_b)/2 \quad (\text{A1}) \\
p_{\theta_a, \theta_b}(1_a, 2_b) &= p_{\theta_a, \theta_b}(2_a, 1_b) = \cos^2(\theta_a - \theta_b)/2.
\end{aligned}$$

APPENDIX B: DEAD TIME CORRECTION DETERMINATION

According to refs. [37, 38] in the case of non-extending dead time, the correction is $\pi_z = 1/(1 + \bar{n}_z D_z/t)$, where \bar{n}_z are the mean number of photons counted in the z

channel, i.e. $\bar{n}_z = \sum_{x_z=1,2} \text{Tr}\{\hat{n}\hat{\rho}_{\text{tot}}^{x_z}\}$ with $\hat{\rho}_{\text{tot}}^{x_z}$ calculated in the absence of dead time D_z , equivalently $\xi_{x_z} = \eta_{x_z}\tau_{x_z}$. We can therefore write down dead time correction in this particular case as

$$\pi_a = \left\{ 1 + \sum_{x_a=1,2} \left[\frac{\sum_{y_b} p_S(x_a, y_b) \eta_{x_a} \tau_{x_a} \alpha_a \lambda_a}{\eta_{x_a} \tau_{x_a} (1 - \alpha_a) \lambda_a / 2 + \lambda_{d,x_a}} \right] D_a \right\}^{-1}$$

and

$$\pi_b = \left\{ 1 + \sum_{x_b=1,2} \left[\frac{\sum_{y_a} p_S(y_a, x_b) \eta_{x_b} \tau_{x_b} \alpha_b \lambda_b}{\eta_{x_b} \tau_{x_b} (1 - \alpha_b) \lambda_b / 2 + \lambda_{d,x_b}} \right] D_b \right\}^{-1}$$

by reminding that, when several devices in series are used, a good approximation is considering the whole apparatus as a black box, with non-extending dead time equal to the largest of dead times of the single compo-

nent [37]. We showed in ref. [38] that π_z provides a satisfactory approximation for $t \gg D_z$.

APPENDIX C: EAVESDROPPING LIMIT FOR WIGNER'S INEQUALITY

We present a similar calculation as in ref. [2] to evaluate the eavesdropping limit for Wigner's inequality, where we assume that Eve prepares each particle of the pairs separately so that each individual particle has a well defined polarization direction, possibly varying from pair to pair. It ensues that the probability $P(\Phi_a, \Phi_b)$ to have Alice's particle in state $|\Phi_a\rangle$, and Bob's particle in state $|\Phi_b\rangle$, where Φ_a and Φ_b are two angles of Eve's polarization preparation. For the density operator of each pair is $\hat{\rho}_{\text{eve}} = \int P(\Phi_a, \Phi_b) |\Phi_a\rangle |\Phi_b\rangle \langle \Phi_b| \langle \Phi_a| d\Phi_a d\Phi_b$, it results

$$W = \int P(\Phi_a, \Phi_b) \left[\cos^2(\Phi_a + \frac{\pi}{6}) \cos^2 \Phi_b + \cos^2 \Phi_a \cos^2(\Phi_b - \frac{\pi}{6}) - \cos^2(\Phi_a + \frac{\pi}{6}) \cos^2(\Phi_b - \frac{\pi}{6}) \right] d\Phi_a d\Phi_b,$$

thus in the case of single channel eavesdropping, $\Phi_b = \Phi_a - \pi/2$, $W = 1/16$, while in the general case Eve has the

total control over the state of individual particle there is no physical boundary condition.

-
- [1] C. Bennett and G. Brassard, in *Proceedings of the IEEE International Conference on Computers, Systems and Signal Processing, Bangalore*, (IEEE, New York 1984), p. 175.
 - [2] A. K. Ekert, Phys. Rev. Lett. **67**, 661 (1991).
 - [3] C. H. Bennett, G. Brassard and N. D. Mermin, Phys. Rev. Lett. **68**, 557 (1992).
 - [4] G. Brassard, N. Lutkenhaus, T. Mor and B. C. Sanders, Phys. Rev. Lett. **85**, 1330 (2000).
 - [5] A. K. Ekert, J. G. Rarity, P. R. Tapster and G. M. Palma, Phys. Rev. Lett. **69**, 1293 (1992).
 - [6] A. V. Sergienko, M. Atature, Z. Walton, G. Jaeger, B. E. A. Saleh and M. C. Teich, Phys. Rev. A **60**, 2622 (1999).
 - [7] T. Jennewein, C. Simon, G. Weihs, H. Weinfurter and A. Zeilinger, Phys. Rev Lett. **84**, 4729 (2000).
 - [8] D. S. Naik, C. G. Peterson, A. G. White, A. J. Berglund and P. G. Kwiat, Phys. Rev. Lett. **84**, 4733 (2000).
 - [9] W. Tittel, J. Brendel, H. Zbinden and N. Gisin, Phys. Rev. Lett. **84**, 4737 (2000).
 - [10] L. Mandel, J. Opt. Soc. Am. B **1**, 108 (1984).
 - [11] E. Jakeman and J. G. Rarity, Opt. Commun. **59**, 219 (1986).
 - [12] J. G. Rarity, P. R. Tapster and E. Jakeman, Opt. Commun. **62**, 201 (1987).
 - [13] J. G. Rarity and P. R. Tapster, Appl. Phys. B **55**, 298 (1992).
 - [14] D. C. Burnham and D. L. Weinberg, Phys. Rev. Lett. **25**, 84 (1970).
 - [15] D. N. Klyshko, *Photons and Nonlinear Optics*, (Gordon and Breach Science Publishers, New York, Amsterdam, 1988).
 - [16] J. G. Rarity, K. D. Ridley and P. R. Tapster, Appl. Opt. **26**, 4616 (1987).
 - [17] A. N. Penin and A. V. Sergienko, Appl. Opt. **30**, 3582 (1991).
 - [18] P. G. Kwiat, A. M. Steinberg, R. Y. Chiao, P. H. Eberhard and M. D. Petroff, Appl. Opt. **33**, 1844 (1994).
 - [19] A. L. Migdall, R. U. Datla, A. V. Sergienko, J. S. Orszak and Y. H. Shih, Metrologia **32**, 479 (1996).
 - [20] S. Castelletto, A. Godone, C. Novero and M. L. Rastello, Metrologia **32**, 501 (1996).
 - [21] M. M. Hayat, A. Joobeur and B. E. A. Saleh, J. Opt. Soc. Am. A **16**, 348 (1999).
 - [22] G. Brida, S. Castelletto, C. Novero and M. L. Rastello, J. Opt. Soc. Am. B **16**, 1623 (1999).
 - [23] G. Brida, S. Castelletto, I. P. Degiovanni, C. Novero and M. L. Rastello, Metrologia **37**, 625 (2000).
 - [24] P. R. Tapster, J. G. Rarity and P. C. M. Owens, Phys. Rev. Lett. **73**, 1923 (1994).
 - [25] W. Tittel, J. Brendel, H. Zbinden and N. Gisin, Phys. Rev. Lett. **81**, 3563 (1998).
 - [26] G. Weihs, T. Jennewein, C. Simon, H. Weinfurter and A. Zeilinger, Phys. Rev. Lett. **81**, 5039 (1998).
 - [27] P. G. Kwiat, A. J. Berglund, J. B. Altepeter and A. G. White, Science **290**, 498 (2000).
 - [28] A. J. Berglund, arXiv:quantph/0010001 v2 (2000).

- [29] N. Boeuf, D. Branning, I. Chaperot, E. Dauler, S. Guerin, G. Jaeger, A. Muller, and A. Migdall, *Opt. Eng.* **39**, 1016 (2000).
- [30] P. G. Kwiat, K. Mattle, H. Weinfurter, A. Zeilinger, A. V. Sergienko and Y. Shih, *Phys. Rev. Lett.* **75**, 4337 (1995).
- [31] It is noteworthy to remind that entangled states may be successfully generated for this purpose by two type I nonlinear crystals [32], so that the general state is $|\psi\rangle = |H_a\rangle|H_b\rangle - \exp[i\phi]|V_a\rangle|V_b\rangle$.
- [32] P. G. Kwiat, E. Waks, A. G. White, I. Appelbaum and P.H. Eberhard, *Phys. Rev. A* **60**, R773 (1999).
- [33] S. Castelletto, I. P. Degiovanni and M. L. Rastello, in *Quantum Communication, Computing, and Measurement 3*, Proceedings of the Fifth International Conference on Quantum Communication, Measurement and Computing, Capri, Italy, edited by P. Tombesi and O. Hirota, (Kluwer Academic, New York, 2001), p. 131.
- [34] J. Perina Jr., O. Haderka and J. Soubusta, *Phys. Rev. A* **64**, 052305 (2001).
- [35] S. Castelletto, I. P. Degiovanni and M. L. Rastello, *J. Opt. Soc. Am. B*, accepted for publication.
- [36] L. Mandel, E. Wolf, *Optical coherence and quantum optics*, (Cambridge University Press, Cambridge, 1995).
- [37] S. Castelletto, I. P. Degiovanni and M. L. Rastello, *Metrologia* **37**, 613 (2000).
- [38] S. Castelletto, I. P. Degiovanni and M. L. Rastello, in *Advanced Mathematical and Computational tools in Metrology V*, edited by P. Ciarlini, M. Cox, E. Filipe, F. Pavese and D. Ricther, (World Scientific Company, Singapore, 2001), p. 41.